



Atypical adsorption of hydrogen on native ultrathin aluminum oxide films

Matic Poberžnik*, Anton Kokalj

Department of Physical and Organic Chemistry, Jožef Stefan Institute, Jamova 39, SI-1000, Ljubljana, Slovenia

ARTICLE INFO

Keywords:

DFT
Ultrathin films
Charge transfer
Hydride
Hydrogen evolution

ABSTRACT

We report on an unusual hydrogen adsorption mode on native ultrathin aluminum-oxide films. Based on systematic density-functional theory (DFT) calculations on a model oxide film of varying thickness — i.e., α -Al₂O₃(001) supported on Al(111) — we show that on ultrathin films, H preferentially adsorbs on surface Al ions instead of O ions, as one would expect from chemical intuition. The so-adsorbed H is in hydride form, and for ultrathin films, it gets the electron charge from Al atoms at the oxide/metal interface. In contrast, for thicker films, this electron transfer ceases, and the charge instead predominantly comes from the surface O ions, making H adsorbed at Al sites inferior to H adsorbed at O sites. We further show that H adsorbed at Al sites can lead to H₂ formation, which we propose to be connected to the experimentally observed hydrogen evolution in pits formed during the pitting corrosion of aluminum, where the protective oxide film has considerably degraded and is very thin.

1. Introduction

Aluminum plays a prominent role in many industries, mainly due to its light weight and excellent corrosion resistance. The latter is a consequence of a spontaneously formed passive oxide film on its surface that provides excellent protection in the pH range from 4 to 8. The thickness of the native oxide film typically ranges from 2 to 3 nm under ambient conditions [1,2]. However, in the case of localized corrosion, its thickness can be considerably reduced. It is known that supported ultrathin films can sometimes exhibit remarkably different properties than their bulk counterparts [3]. A prototypical example is the case of Au adatoms on MgO(100) supported on Mo(100) [4] where the gold adatoms are negatively charged and adsorb more strongly and at a different surface site than on the bulk counterpart [4]. However, electron transfer across ultrathin oxide films is not limited to Au and has been observed for other adsorbates, such as O₃, Cl₂, NO₂, H₂O₂, and O₂ deposited on supported ultrathin films [1,5–8].

Such charge transfer was originally attributed to direct tunneling of electrons from the metal to the empty states of the electronegative adsorbate, the only provision being that these states are located below the Fermi level of the metal [4,9]. However, it was later shown that the charge originates from the oxide/metal interface, resulting in a long-range chemical bond mechanism that can affect the adsorption site preference and enhance the bond strength in comparison to the

surfaces of bulk oxides [10–12]. This effect was attributed to the concerted action of several contributions, the relative importance of each depending on the system composition, but the long-range nature of the phenomenon was ascribed to electrostatic polarization. Additionally, charge transfer from the adsorbate to the oxide/metal interface has also been reported [13,14]. This charge transfer was found to change the H₂ dissociation mechanism from heterolytic to homolytic on Au supported ultrathin MgO(001) films [13]. On the other hand, for the adsorption of water on Ag(100) supported ultrathin MgO, the metal support enhanced the adsorption energies of isolated OH and H, due to the charge transfer from the metal/oxide interface to OH and from H to the interface [14].

In this article, we show that contrary to chemical intuition, H prefers to bond to Al cation sites instead of O anion sites on native ultrathin aluminum-oxide films. By systematically varying the thickness of a model oxide film — i.e., α -Al₂O₃(001) supported on Al(111) — we show that this behavior is specific to ultrathin oxide films and does not occur on bulk oxide surfaces and films thicker than about 2 nm. We demonstrate that for ultrathin films, H is in hydride form, with its charge originating from the oxide/metal interface. We propose that this bonding mode can lead to the hydrogen evolution reaction, which has been observed in pits during localized corrosion of aluminum [15]. This reaction is known as the negative difference effect (NDE) because

* Corresponding author.

E-mail address: matic.poberznik@ijs.si (M. Poberžnik).

<https://doi.org/10.1016/j.surfin.2025.105742>

Received 27 August 2024; Received in revised form 16 December 2024; Accepted 2 January 2025

Available online 15 January 2025

2468-0230/© 2025 The Authors. Published by Elsevier B.V. This is an open access article under the CC BY license (<http://creativecommons.org/licenses/by/4.0/>).

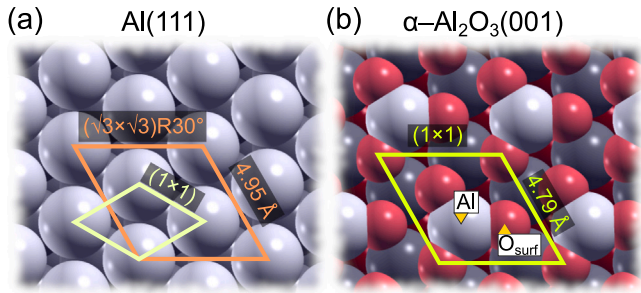


Fig. 1. Topviews of Al(111) and α -Al₂O₃(001); the structures are visualized with atomic radii in order to enhance the readability, although for the oxide film, the use of ionic radii would be physically more appropriate. The (1 × 1) cells for each surface are indicated. The $(\sqrt{3} \times \sqrt{3})R30^\circ$ supercell of Al(111), with a lattice parameter of 4.95 Å, has the same shape and a similar size to the (1 × 1) cell of α -Al₂O₃(001), which has a lattice parameter of 4.79 Å. The lattice mismatch is thus 3.3%. Hence, the slabs were merged commensurately, such that the lattice parameter of Al(111) was imposed with a five layer thick Al(111) slab acting as the metallic support. The thickness of the vacuum region was set to at least 15 Å and the dipole correction of Bengtsson [36] was applied.

its rate counterintuitively increases with increasing anodic polarization on metals, such as Al, Mg, and their alloys [16–22].

2. Technical details

2.1. Computational details

DFT calculations were performed with the PWscf code from the Quantum ESPRESSO distribution [23,24] using the generalized-gradient approximation (GGA) of Perdew–Burke–Ernzerhof (PBE) [25]. We used the pseudo-potential method with ultra-soft pseudo-potentials [26,27]. Kohn–Sham orbitals were expanded in a plane wave basis set up to a kinetic energy cutoff of 35 Ry (280 Ry for the charge-density cutoff). A Methfessel–Paxton smearing [28] of 0.03 Ry was used, whereas the Brillouin zone (BZ) integrations were performed with the special-point technique [29]. The Bader charge analysis was performed by generating charge densities with single point self-consistent-field calculations of US-PP optimized structures using the PAW (projector-augmented-wave) potentials [30,31] and a 1000 Ry kinetic energy cutoff for the charge density and then computing the Bader charges using the bader program [32,33]. Molecular graphics were produced by the XCRYSDEN graphical package [34].

2.2. The model of the supported oxide thin film

We chose a model of the aluminum-oxide film based on the (001) slab of α -Al₂O₃ supported on Al(111), for which the thickness can be systematically varied. A similar model was used by Baran et al. for the study of limiting oxide thickness on aluminum [7].

On the vacuum side of the pristine oxide film, there are three possible terminations of α -Al₂O₃(001), which we designate as α -Al₂O₃^{Al_t}, α -Al₂O₃^{stoch}, and α -Al₂O₃^{O_t}, depending on where the crystal structure is cleaved. The hexagonal unit cell of the α -Al₂O₃(001) slab displays a repeating pattern of –O–Al1–Al2– in the [001] direction, where O represents a layer of oxygen ions, whereas Al1 and Al2 designate layers of aluminum ions. If the slab is cut between Al2–O, then the slab is Al-terminated and it is designated as α -Al₂O₃^{Al_t}. If it is cut between Al1–Al2, the resulting slab is stoichiometric (labeled as α -Al₂O₃^{stoch}). Instead, if it is cut between O–Al1, then the slab is O-terminated and it is designated as α -Al₂O₃^{O_t}. The topview of the α -Al₂O₃^{stoch}(001) surface model is shown in Fig. 1b, whereas the sideview for the four oxygen layer thick α -Al₂O₃^{stoch}(001) slab is presented in Fig. 2a. When the (hydroxyl free) oxide surface is in contact with an oxygen atmosphere, the α -Al₂O₃^{stoch}(001) termination displays the lowest surface free energy for all accessible values of oxygen chemical potential. Its calculated surface energy of 130 meV/Å² agrees with calculations from Ref. [35].

This termination was used to model the vacuum/oxide interface. The topmost layer of the pristine oxide film contains a layer of aluminum ions, designated Al, and a layer of oxygen ions, designated O_{surf} (cf. Figs. 1b and 2.) The oxygen ions of the first subsurface layer are designated as O_{sub} (cf. Fig. 2).

On the side of the oxide/metal interface, we note that the $(\sqrt{3} \times \sqrt{3})R30^\circ$ supercell of Al(111) has the same shape and a similar lattice parameter (4.95 Å) as the (1 × 1) cell of α -Al₂O₃(001) (4.79 Å); the lattice mismatch is thus 3.3%. Hence, the slabs were merged commensurately, such that the lattice parameter of Al(111) was imposed with a five layer thick Al(111) slab acting as the metallic support. The thickness of the vacuum region was set to at least 15 Å and the dipole correction of Bengtsson [36] was applied.

The BZ integrations were performed with a 6 × 6 × 1 uniformly shifted k-mesh for the (1 × 1)- α -Al₂O₃(001)/Al(111) model, and 6 × 3 × 1 and 3 × 3 × 1 k-meshes for the corresponding (1 × $\sqrt{3}$) and (2 × 2) supercells. In matrix notation, the (1 × $\sqrt{3}$) supercell is described as $\begin{pmatrix} 1 & 0 \\ 1 & 2 \end{pmatrix}$; the lengths of the two supercell vectors are $A = 1a$ and $B = \sqrt{3}a$, where a is the length of the unit-cell vectors; hence, the label (1 × $\sqrt{3}$). Additionally, the bottom two layers of the Al(111) slab were kept fixed during structural relaxations.

The structure of the oxide/metal interface was determined by following the approach outlined by Finnis [37] for two component systems in which the stoichiometry of the oxide is accounted for and excess aluminum ions are treated as part of the bulk metal. The interfacial surface free energy (γ_{intf}) was calculated as:

$$\gamma_{\text{intf}} = \frac{1}{2A}(G_{\text{ox/met}} - N_{\text{ox}}\mu_{\text{ox}} - N_{\text{met}}\mu_{\text{met}}) - \gamma_{\text{Al(111)}}, \quad (1)$$

where $G_{\text{ox/met}}$ was approximated by the total energy of the metal/oxide/metal system with the oxide film placed between the two metallic slabs in such a way that the interface between metal and oxide was equivalent on both sides, while the metallic slabs were separated by a vacuum. N_{ox} is the number of Al₂O₃ units in the oxide film and μ_{ox} is approximated by the total energy of an Al₂O₃ unit in bulk α -Al₂O₃. N_{met} is the total number of metallic atoms per supercell and μ_{met} is approximated by the total energy of aluminum atom in the bulk metal. A is the area of the supercell and the factor $\frac{1}{2}$ stems from the fact that the oxide slab is in contact with the metal on both sides. Note that the additional $\gamma_{\text{Al(111)}}$ term is the surface energy of the Al(111) slab with a value of 40 meV/Å². It is needed because each metallic slab is terminated by vacuum.

Evaluating the stability of the interface with Eq. (1), we find that the lowest interfacial energy, 99 meV/Å², is found for α -Al₂O₃^{Al_t}(001) with the terminating Al atoms bound at the hcp site of Al(111). It is followed by α -Al₂O₃^{stoch}(001), with a value of 129 meV/Å², and the highest value is obtained for the α -Al₂O₃^{O_t}(001) case, with 151 meV/Å². Thus, we chose the α -Al₂O₃^{Al_t}(001) termination to construct the oxide/metal interface. This interface consists of two aluminum atoms, designated as Al_{up} and Al_{down} (Fig. 2b). Al_{down} is bound to the hcp site of Al(111) and is closer to the metal support, whereas Al_{up} is closer to the oxide film. Additionally, the Al atoms of the topmost metal layer, closest to the two interface atoms are designated as Al_{met}.

2.3. Reaction energies and reaction Gibbs energies

The reaction energy (ΔE) is defined as the difference between the sum of the total energies of products and reactants:

$$\Delta E = \sum_i^{\text{products}} E_i - \sum_j^{\text{reactants}} E_j. \quad (2)$$

For a limited subset of calculations reported in this work, we also calculated the reaction Gibbs energies (ΔG) at $T = 298.15$ K and a partial pressure of $p = 1$ atm for gaseous species, where ΔG is defined analogously to ΔE in Eq. (2). For these calculations, the k-point

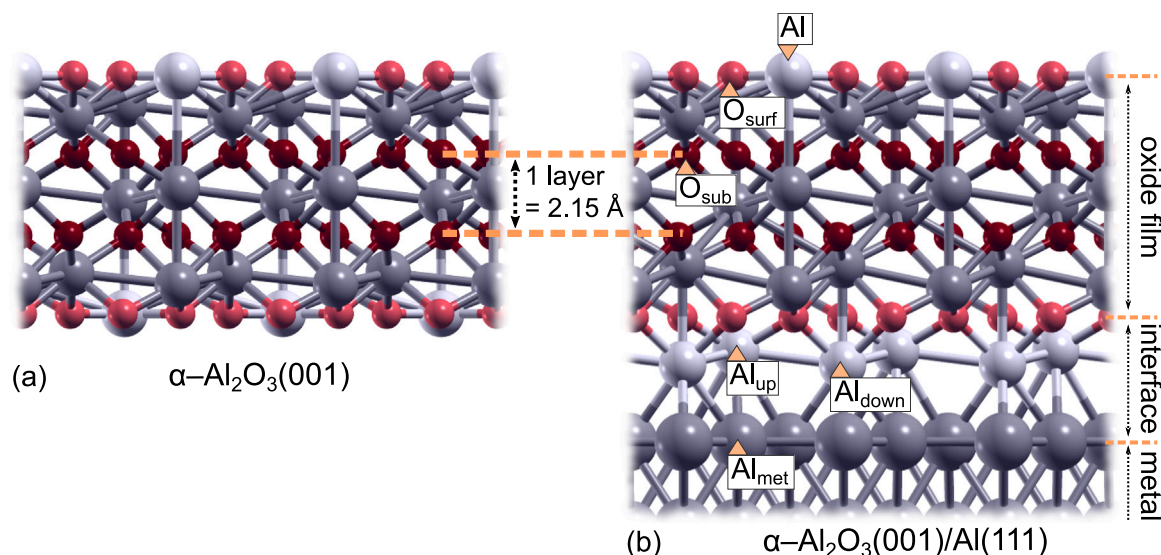


Fig. 2. Sideview of a four oxygen layer thick (a) standalone α - $\text{Al}_2\text{O}_3^{\text{stoich}}(001)$ slab and (b) α - $\text{Al}_2\text{O}_3(001)$ slab supported on $\text{Al}(111)$. Note that the terminations correspond to α - $\text{Al}_2\text{O}_3^{\text{stoich}}$ at the vacuum/oxide interface and to α - $\text{Al}_2\text{O}_3^{\text{Al}}$ at the oxide/metal interface. Atom designations used throughout the text are stated.

sampling was reduced to a $4 \times 4 \times 1$ k-mesh for the (1×1) - α - $\text{Al}_2\text{O}_3(001)/\text{Al}(111)$ model, and all degrees of freedom were relaxed. The vibrational frequencies were evaluated with the PHonon code at the Γ q-point [38]. Vibrational contributions to thermal energy and entropy were calculated using the quasi-harmonic approximation of Cramer–Thrular [39], with the vibrational frequencies below 100 cm^{-1} raised to 100 cm^{-1} to remedy the breakdown of the harmonic oscillator model for low-frequency vibrational modes.

For gaseous species (hydrogen gas), the contributions from translational and rotational modes were considered using the ideal-gas approximation and the rigid-rotor model, respectively, whereas for the surfaces and adsorbates thereon, only the vibrational contribution to thermal energy and entropy was taken into account, and the pV term was neglected.

3. Results and discussion

3.1. The binding of H on the supported thin film

Using the model of the supported oxide described in Section 2.2, we investigated the adsorption of hydrogen on oxide films of different thicknesses by the following reaction:



where $*$ indicates a free adsorption site, and $\text{H}*$ stands for a chemisorbed H atom. Two sites, designated as Al and O_{surf} (see Fig. 1b), were considered on the supported and non-supported oxide films. How the reaction energy changes with oxide thickness for the highest considered coverage, corresponding to (1×1) overlayers on α - $\text{Al}_2\text{O}_3(001)$, is summarized in Fig. 3b. Notice that adsorption at O_{surf} sites is similar for both the supported and non-supported films and it remains constant for all considered oxide thicknesses, with an endothermic value of approximately 1.6 eV per H atom. In contrast, adsorption at Al sites displays remarkably different behavior on the two films. On the supported oxide films, the adsorption energy for H at the Al site depends considerably on the oxide thickness, about -0.8 eV for film thicknesses below 7 \AA (corresponding to 4 oxygen layers) and endothermic for thicker films, reaching the value of the O_{surf} site at a film thickness of approximately 30 \AA . On the non-supported film, its value at the Al site is almost independent on the film thickness, having an endothermic value of about 2 eV. Additionally, we considered heterolytic adsorption of H_2 , where both sites are occupied

simultaneously (labeled as $\text{H}_{\text{Al}} + \text{H}_{\text{O}_{\text{surf}}}$), resulting in two adsorbed H atoms per (1×1) supercell (see Fig. 3a). This adsorption mode is nearly athermic, with a ΔE value of about -0.1 eV/H-atom . It is similar for both the supported and non-supported model of the oxide film and remains approximately constant for all considered film thicknesses. This adsorption mode is therefore thermodynamically preferred on non-supported and thicker supported oxide films.

Further, we investigated how the reaction energy for hydrogen adsorption depends on coverage. The results shown in Fig. 3c reveal that the binding is even more exothermic at lower coverage (-1.1 eV per H atom for the (2×2) overlayer of the thinnest film considered herein). As the oxide-film thickness increases, the binding becomes less exothermic, but the change is considerably more gradual than that at full coverage. Specifically, the binding becomes less favorable than the most stable identified $\text{H}_{\text{Al}} + \text{H}_{\text{O}_{\text{surf}}} - (1 \times \sqrt{3})$ structure in Fig. 3c for oxide films thicker than about 10 \AA for the $(1 \times \sqrt{3})$ overlayer and about 20 \AA for the less dense (2×2) overlayer. These observations thus indicate that both factors, oxide thickness and adatom coverage are to be considered for the binding of H on Al sites. Furthermore, our analysis indicates that the change in adsorption energy as a function of the oxide-film thickness is more gradual for lower coverages due to lower surface charge density. This effect is reminiscent of the work required for charging a parallel plate capacitor, which is proportional to $q^2 d/A$, where q is the charge per supercell, d is the interplate distance, and A is the supercell area. In particular, by linear fitting the ΔE values for thin films of the three considered coverages, one obtains slopes that are inversely proportional to the cell area (Fig. S1 in the Supplementary material).

It is worth mentioning that H prefers to bind to Al sites also on other models of native ultrathin aluminum-oxide films, provided that Al ions are present on the surface, such as stoichiometric α - $\text{Al}_2\text{O}_3^{\text{stoich}}/\text{Al}(111)$ and the one employed in our previous study [40] that is based on Ref. [41].

Since H binds to aluminum cations on thin supported oxide films, it should be negatively charged (in hydride form). To verify this assumption and to establish from where its charge originates, we used Bader charge analysis before and after hydrogen adsorption on the supported oxide films, and the results are summarized in Fig. 4. The analysis shows that H is indeed negatively charged, with a charge of about -0.9 for ultrathin films and about -0.7 for thicker films. To establish from where this charge originates, we first examine the aluminum ions at the oxide/metal interface, designated Al_{up} and Al_{down}

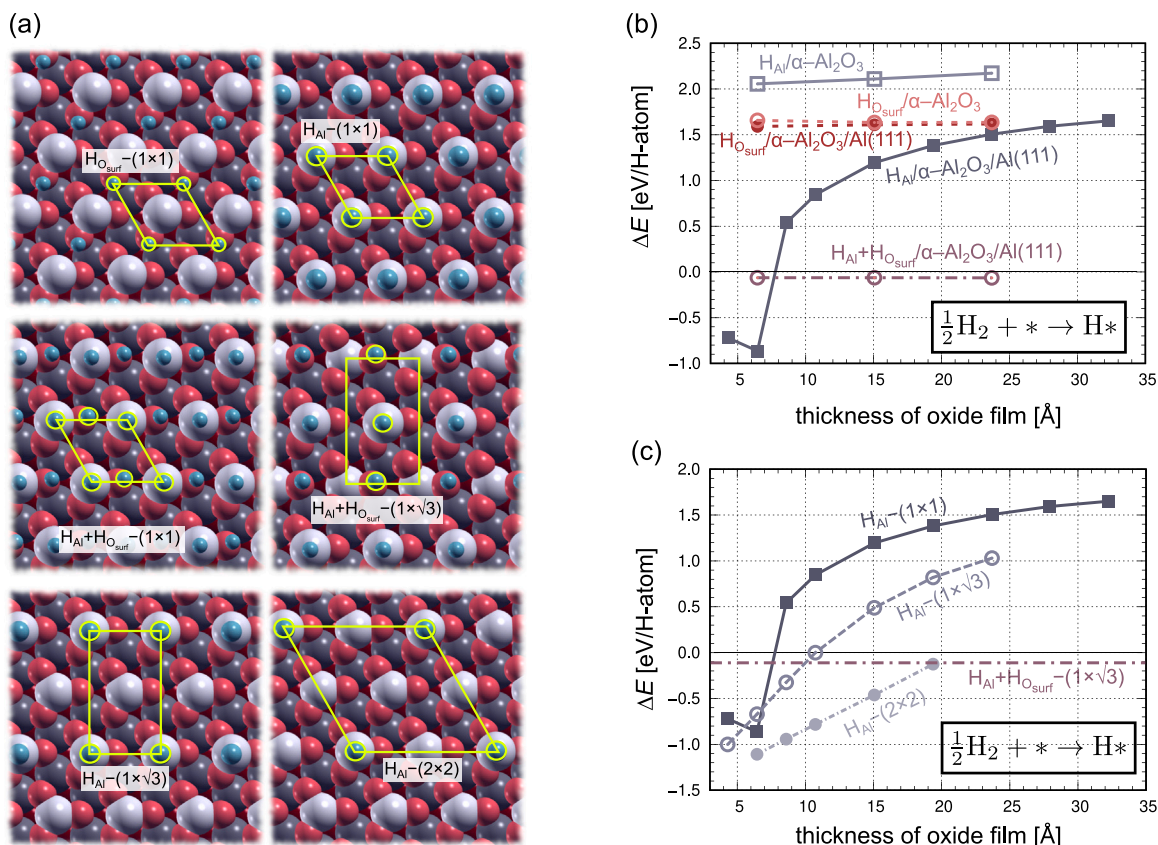


Fig. 3. (a) Topviews of considered H overlayers. (b) ΔE for H adsorption (per H atom), reaction (3), for different sites on the supported and non-supported oxide films. (c) ΔE for different coverages of H at the Al site against oxide thickness (beware that the ordinate axes in (b) and (c) differ). Note that for very thin films, the adsorption of H at the Al site is exothermic, and the degree of exothermicity decreases with increasing oxide thickness, with the thickness at which it becomes endothermic depending on the coverage.

in Fig. 2. From Fig. 4a, it is evident that for ultrathin films, the two interface Al ions become considerably more positively charged after adsorption of H, while for thicker films, their charge is similar to that before adsorption. To demonstrate this observation more clearly, we calculated the adsorption induced change in charge (Δq) for the ions that are specifically indicated in Fig. 2b, i.e.:

$$\Delta q = q(\text{after}) - q(\text{before}). \quad (4)$$

These values are plotted in Fig. 4b. For thicker films, the summed difference for the two interface Al ions:

$$\Delta q_{\text{intf}} = \Delta q_{Al_{up}} + \Delta q_{Al_{down}}, \quad (5)$$

becomes close to zero, while $\Delta q_{O_{surf}}$ becomes substantial. This indicates that for thin films, the majority of charge stems from the oxide/metal interface, while for thicker films, it comes from the surface oxygen ions. This is schematically depicted in Fig. 4d. Our analysis also reveals that the metal slab underneath the oxide films, i.e., Al_{met} atoms beneath the two interface Al ions hardly participate in charge transfer. Further, by taking the sum of charge differences of the considered subset of substrate ions (Δq_{sel}), the charge on H is reproduced remarkably well, indicating that (almost) all sources of H charge are accounted for.

It is therefore evident that the majority of charge on H for ultrathin films is transferred from the oxide/metal interface Al atoms. Consequently, the amount of charge transferred from the oxide/metal interface depends on the oxide-film thickness and ceases for thick films. However, H adsorbed at the Al site is negatively charged irrespective of the film thickness (Fig. 4a), implying that the charge originates from elsewhere for thick films. Our analysis reveals that it comes mainly from the O_{surf} and O_{sub} ions.

3.2. Implications and connection to hydrogen evolution

Let us explore the possible implications of H binding to Al ions on ultrathin films for the hydrogen evolution reaction. To this end, we consider the non-dissociative and dissociative adsorption of water on the (supported) oxide films. Non-dissociative adsorption can be described by the following reaction:



Our calculations show that the reaction energy for the non-dissociative adsorption of water does not depend on oxide thickness and remains constant at about -1 eV for all investigated thicknesses. This value is in line with that obtained by other groups on the $\alpha-Al_2O_3(001)$ surface [42,43].

The second possibility is the dissociative adsorption of water, described by the following reaction:



where the dissociated H can bind to either the O_{surf} or the Al site, i.e.:



and



We investigated how the reaction energy for dissociative adsorption of water depends on the oxide-film thickness and adsorbate coverage (Fig. 5). Our results indicate that the reaction energy for H adsorbed to O_{surf} , reaction (8), does not depend on the oxide thickness and displays a ΔE value of about -1.4 eV. This value is similar to that obtained by other groups for non-supported $\alpha-Al_2O_3(001)$ [44,45] and is more exothermic than the non-dissociative adsorption energy and therefore

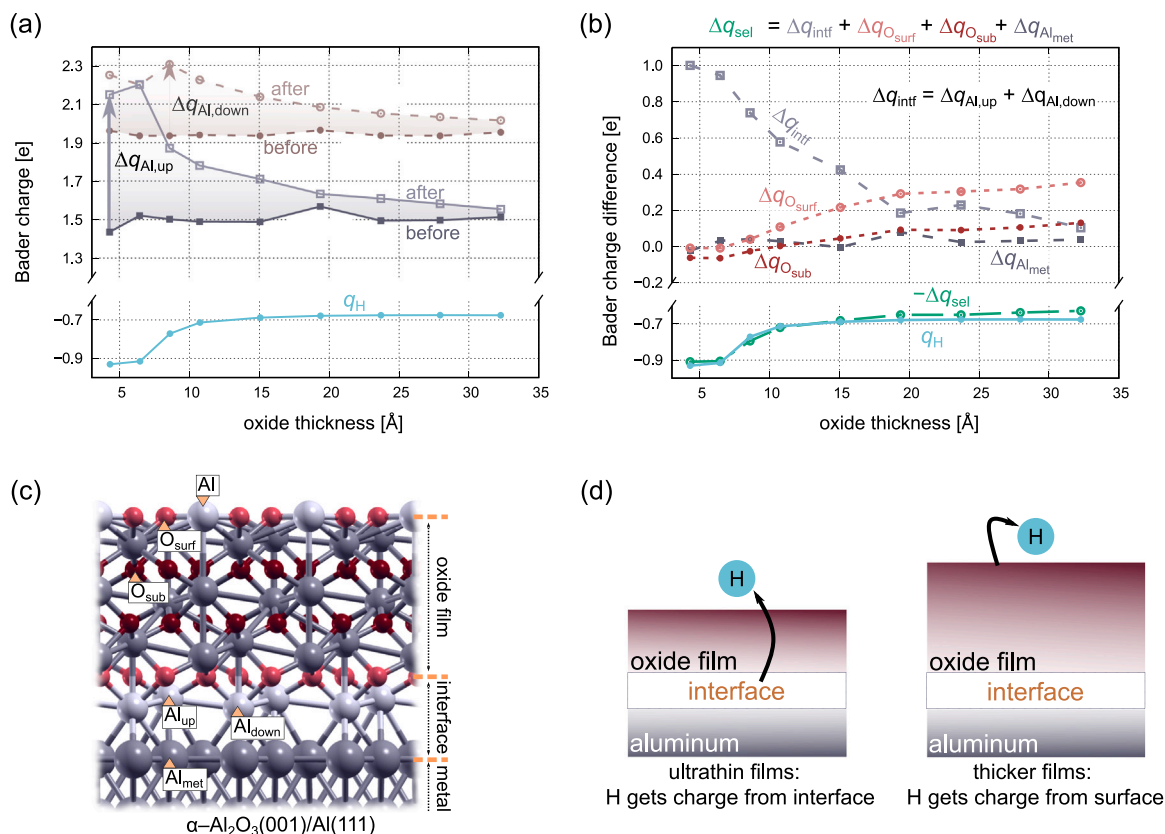


Fig. 4. (a) Bader charge (q) of the adsorbed H adatom and Al ions at the oxide/metal interface before and after H adsorption as a function of oxide-film thickness. The adsorption induced change in charge, $\Delta q = q(\text{after}) - q(\text{before})$, is indicated by arrows for the two interface Al ions. (b) Δq for characteristic substrate ions versus oxide thickness; Δq_{intf} corresponds to the sum of the interface aluminum ions and Δq_{sel} to the sum of considered substrate ions, as indicated on the plot. (c) Sideview of a four oxygen layer thick $\alpha\text{-Al}_2\text{O}_3/\text{Al}(111)$ slab with atom labels. (d) A scheme depicting the main result of Bader charge analysis, i.e., for thin films, the excess H charge stems mainly from the interface Al ions, while for thicker films, it predominantly comes from the O_{surf} ions and to lesser extent from the O_{sub} ions.

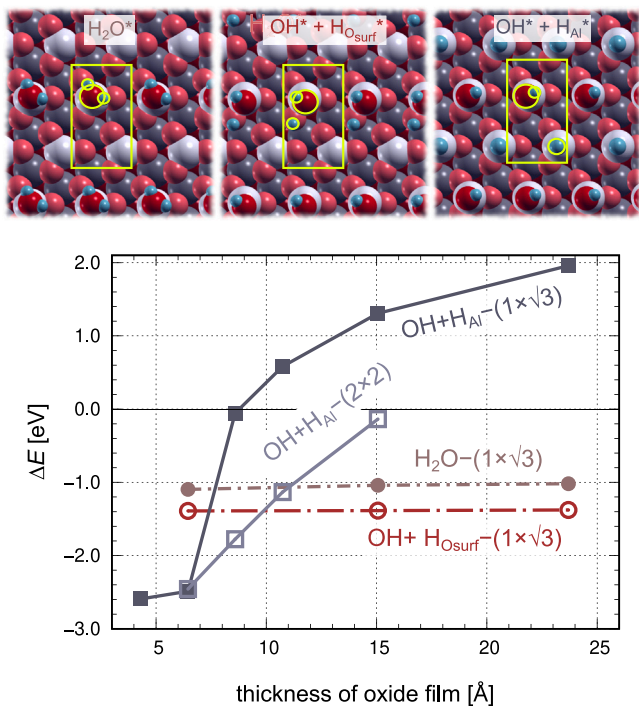


Fig. 5. Top: the topviews of the different adsorption modes of water in a $(1 \times \sqrt{3})$ supercell. Bottom: dependence of ΔE for the three possible H_2O adsorption modes on the thickness of the oxide film on Al(111). The coverage corresponds to one H_2O molecule per $(1 \times \sqrt{3})$ or (2×2) supercell.

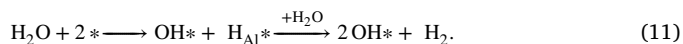
thermodynamically favored.

In contrast to above considered reactions (6) and (8), where the ΔE values are insensitive to oxide-film thickness, the reaction energies for reaction (9) with H at Al sites, depends strongly on the oxide thickness (Fig. 5). For ultrathin films this adsorption mode is the most exothermic, with a value of -2.6 eV per H_2O molecule for both considered coverages. However, the exothermicity of this mode rapidly decreases with increasing oxide-film thickness and it becomes inferior to the other two modes for thicknesses above about 7 and 10 Å for the coverages corresponding to $(1 \times \sqrt{3})$ and (2×2) supercells, respectively.

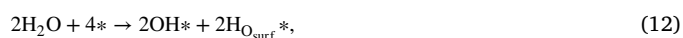
Next, we also examined the possibility of the adsorption of an additional water molecule per supercell displacing the adsorbed H, according to the following reaction:



Because the H adsorbed at Al sites becomes increasingly unfavorable as the thickness of the oxide film increases (cf. Fig. 5), it is more instructive to consider the cumulative reaction, which can be written as:



How the reaction Gibbs energy (ΔG at $p = 1$ atm and $T = 298$ K) changes for the first step and the overall reaction (11) with respect to oxide-film thickness is plotted in Fig. 6; note that only the $(1 \times \sqrt{3})$ supercell is considered. The second step of reaction (11) is always exergonic by about 1.0 eV indicating that it is favorable for water to displace H adsorbed on Al sites, forming H_2 . However, above oxide-film thickness of about 7 Å, the reaction (11) becomes inferior to the following reaction:



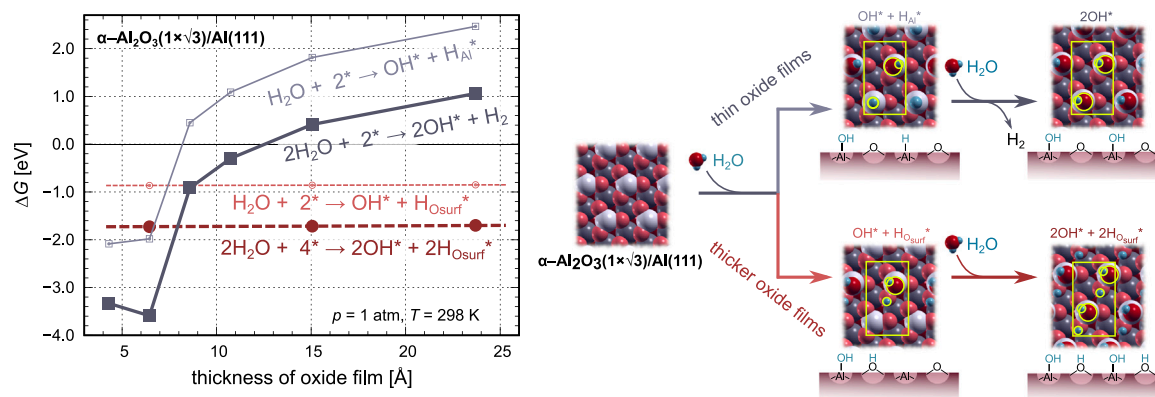


Fig. 6. The dependence of Gibbs reaction energies (ΔG at $p = 1$ atm and $T = 298$ K) for the first step of reaction (11), the cumulative reaction (11), and reaction (12) on oxide-film thickness. The reactions schemes are shown on the right, and the coverage corresponds to the $(1 \times \sqrt{3})$ supercell. Note that at this coverage, reaction (11) is the most exergonic only for oxide thicknesses below about 7 Å, indicating that hydrogen evolution will only take place on ultrathin films, while on thicker films, binding to O_{surf} ions is preferred.

indicating that H_2 evolution would not take place (cf. Fig. 6). Based on Figs. 3c and 5, we can argue that at lower adsorbate coverages, the limiting oxide-film thicknesses where the H_2 evolution would cease are thicker. Despite this consideration, for H_2 evolution to occur, sufficiently thin supported oxide films are required. Such a conclusion aligns with the trend emerging from experimental studies supporting the partial passive film breakdown mechanism for the hydrogen evolution reaction [17,19,20].

4. Conclusions

We performed a DFT based investigation of the unusual hydrogen adsorption on ultrathin aluminum-oxide films supported on aluminum. In particular, we found that H prefers to bond to surface Al ions in hydride form. The Bader charge analysis revealed that the charge on H is transferred from the oxide/metal interface. Consequently, this charge transfer depends on the thickness of oxide film and ceases for thicker films. We further demonstrated that due to this anomalous adsorption-site preference, hydrogen evolution during water dissociation is thermodynamically favorable for ultrathin films; in contrast, for thicker oxide films, water dissociation results in surface hydroxylation. Our calculations thus corroborate the experimentally proposed passive film breakdown mechanism for the observed hydrogen evolution in the pits formed during the pitting corrosion of aluminum and provide an atomic-level insight on how such a reaction can occur.

CRedit authorship contribution statement

Matic Poberžnik: Writing – review & editing, Writing – original draft, Visualization, Methodology, Investigation, Formal analysis, Conceptualization. **Anton Kokalj:** Writing – review & editing, Supervision, Investigation, Formal analysis, Conceptualization.

Declaration of competing interest

The authors declare that they have no known competing financial interests or personal relationships that could have appeared to influence the work reported in this paper.

Acknowledgment

This work has been supported by the Slovenian Research and Innovation Agency (Grant No. P2-0393).

Appendix A. Supplementary data

Supplementary material related to this article can be found online at <https://doi.org/10.1016/j.surfin.2025.105742>.

Data availability

Data will be made available on request.

References

- [1] I. Popova, V. Zhukov, J. Yates, Depth-dependent electrical impedance distribution in Al_2O_3 films on Al(111) detection of an inner barrier layer, *Langmuir* 16 (26) (2000) 10309–10314, <http://dx.doi.org/10.1021/la001009h>.
- [2] J. Evertsson, F. Bertram, F. Zhang, L. Rullik, L. Merte, M. Shipilin, M. Soldemo, S. Ahmadi, N. Vinogradov, F. Carlà, J. Weissenrieder, M. Göthelid, J. Pan, A. Mikkelsen, J.-O. Nilsson, E. Lundgren, The thickness of native oxides on aluminum alloys and single crystals, *Appl. Surf. Sci.* 349 (2015) 826–832, <http://dx.doi.org/10.1016/j.apsusc.2015.05.043>.
- [3] H.-J. Freund, G. Pacchioni, Oxide ultra-thin films on metals: new materials for the design of supported metal catalysts, *Chem. Soc. Rev.* 37 (2008) 2224–2242, <http://dx.doi.org/10.1039/B718768H>.
- [4] G. Pacchioni, L. Giordano, M. Baistrocchi, Charging of metal atoms on ultrathin MgO/Mo(100) films, *Phys. Rev. Lett.* 94 (2005) 226104, <http://dx.doi.org/10.1103/PhysRevLett.94.226104>.
- [5] D. Costa, T. Ribeiro, F. Mercuri, G. Pacchioni, P. Marcus, Atomistic modeling of corrosion resistance: A first principles study of O_2 reduction on the Al(111) surface covered with a thin hydroxylated alumina film, *Adv. Mater. Interfaces* 1 (3) (2014) 1300072, <http://dx.doi.org/10.1002/admi.201300072>.
- [6] C. Ocal, S. Ferrer, N. García, Cabrera-Mott mechanism for oxidation of metals explains diffusion of metallic atoms through thin defective oxide layers, *Surf. Sci.* 163 (2) (1985) 335–356, [http://dx.doi.org/10.1016/0039-6028\(85\)91064-7](http://dx.doi.org/10.1016/0039-6028(85)91064-7).
- [7] J.D. Baran, H. Grönbeck, A. Hellman, Mechanism for limiting thickness of thin oxide films on aluminum, *Phys. Rev. Lett.* 112 (14) (2014) 146103, <http://dx.doi.org/10.1103/PhysRevLett.112.146103>.
- [8] H.V. Thang, S. Tosoni, G. Pacchioni, Evidence of charge transfer to atomic and molecular adsorbates on ZnO/X(111) (X= Cu, Ag, Au) ultrathin films. relevance for Cu/ZnO catalysts, *ACS Catal.* 8 (5) (2018) 4110–4119, <http://dx.doi.org/10.1021/acscatal.7b03896>.
- [9] G. Pacchioni, H. Freund, Electron transfer at oxide surfaces. The MgO paradigm: from defects to ultrathin films, *Chem. Rev.* 113 (6) (2013) 4035–4072, <http://dx.doi.org/10.1021/cr3002017>.
- [10] H. Grönbeck, Mechanism for NO_2 charging on metal supported MgO, *J. Phys. Chem. B* 110 (24) (2006) 11977–11981, <http://dx.doi.org/10.1021/jp0616415>.
- [11] A. Hellman, H. Grönbeck, Activation of Al_2O_3 by a long-ranged chemical bond mechanism, *Phys. Rev. Lett.* 100 (2008) 116801, <http://dx.doi.org/10.1103/PhysRevLett.100.116801>.
- [12] P. Frondelius, A. Hellman, K. Honkala, H. Häkkinen, H. Grönbeck, Charging of atoms, clusters, and molecules on metal-supported oxides: A general and long-ranged phenomenon, *Phys. Rev. B* 78 (2008) 085426, <http://dx.doi.org/10.1103/PhysRevB.78.085426>.
- [13] H.-Y.T. Chen, L. Giordano, G. Pacchioni, From heterolytic to homolytic H_2 dissociation on nanostructured MgO(001) films as a function of the metal support, *J. Phys. Chem. C* 117 (20) (2013) 10623–10629, <http://dx.doi.org/10.1021/jp4037588>.
- [14] K. Honkala, A. Hellman, H. Grönbeck, Water dissociation on MgO/Ag(100): Support induced stabilization or electron pairing? *J. Phys. Chem. C* 114 (15) (2010) 7070–7075, <http://dx.doi.org/10.1021/jp9116062>.

- [15] G.S. Frankel, S. Fajardo, B.M. Lynch, Introductory lecture on corrosion chemistry: a focus on anodic hydrogen evolution on Al and Mg, *Faraday Discuss.* 180 (2015) 11–33, <http://dx.doi.org/10.1039/C5FD00066A>.
- [16] C.B. Barger, R.C. Benson, Analysis of the gases evolved during the pitting corrosion of aluminum in various electrolytes, *J. Electrochem. Soc.* 127 (11) (1980) 2528, <http://dx.doi.org/10.1149/1.2129511>.
- [17] C. Laurent, F. Scenini, T. Monetta, F. Bellucci, M. Curioni, The contribution of hydrogen evolution processes during corrosion of aluminium and aluminium alloys investigated by potentiodynamic polarisation coupled with real-time hydrogen measurement, *Npj Mater. Degrad.* 1 (6) (2017) 1–7, <http://dx.doi.org/10.1038/s41529-017-0011-4>.
- [18] M.A. Coronel-García, J.G. Salazar-Barrera, J.J. Malpica-Maldonado, A.L. Martínez-Salazar, J.A. Melo-Banda, Hydrogen production by aluminum corrosion in aqueous hydrochloric acid solution promoted by sodium molybdate dihydrate, *Int. J. Hydrog. Energy* 45 (26) (2020) 13693–13701, <http://dx.doi.org/10.1016/j.ijhydene.2020.01.122>.
- [19] M. Curioni, F. Scenini, The mechanism of hydrogen evolution during anodic polarization of aluminium, *Electrochim. Acta* 180 (2015) 712–721, <http://dx.doi.org/10.1016/j.electacta.2015.08.076>.
- [20] Y. Yu, Y. Li, New insight into the negative difference effect in aluminium corrosion using in-situ electrochemical ICP-OES, *Corros. Sci.* 168 (2020) 108568, <http://dx.doi.org/10.1016/j.corsci.2020.108568>.
- [21] E. Mysliu, O. Lunderb, A. Erbe, Role of aluminium hydrides in localised corrosion of aluminium revealed by operando Raman spectroscopy, *Phys. Chem. Chem. Phys.* 25 (16) (2023) 11845–11857, <http://dx.doi.org/10.1039/D3CP00522D>.
- [22] C.D. Taylor, A first-principles surface reaction kinetic model for hydrogen evolution under cathodic and anodic conditions on magnesium, *J. Electrochem. Soc.* 163 (9) (2016) C602, <http://dx.doi.org/10.1149/2.1171609jes>.
- [23] P. Giannozzi, S. Baroni, N. Bonini, M. Calandra, R. Car, C. Cavazzoni, D. Ceresoli, G.L. Chiarotti, M. Cococcioni, I. Dabo, A. Dal Corso, S. de Gironcoli, S. Fabris, G. Fratesi, R. Gebauer, U. Gerstmann, C. Gougoussis, A. Kokalj, M. Lazzeri, L. Martin-Samos, N. Marzari, F. Mauri, R. Mazzarello, S. Paolini, A. Pasquarello, L. Paulatto, C. Sbraccia, C. Scandolo, G. Sclauzero, A.P. Seitsonen, A. Smogunov, P. Umari, R.M. Wentzcovitch, Quantum ESPRESSO: a modular and open-source software project for quantum simulations of materials, *J. Phys.: Condens. Matter.* 21 (39) (2009) 395502, <http://dx.doi.org/10.1088/0953-8984/21/39/395502>, code available from <http://www.quantum-espresso.org/>.
- [24] P. Giannozzi, O. Andreussi, T. Brumme, O. Bunau, M.B. Nardelli, M. Calandra, R. Car, C. Cavazzoni, D. Ceresoli, M. Cococcioni, N. Colonna, I. Carnimeo, A.D. Corso, S. de Gironcoli, P. Delugas, R. DiStasio, A. Ferretti, A. Floris, G. Fratesi, G. Fugallo, R. Gebauer, U. Gerstmann, F. Giustino, T. Gorni, J. Jia, M. Kawamura, H.-Y. Ko, A. Kokalj, E. Küçükbenli, M. Lazzeri, M. Marsili, N. Marzari, F. Mauri, N.L. Nguyen, H.-V. Nguyen, A.O. de-la Roza, L. Paulatto, S. Poncè, D. Rocca, R. Sabatini, B. Santra, M. Schlipf, A.P. Seitsonen, A. Smogunov, I. Timrov, T. Thonhauser, P. Umari, N. Vast, X. Wu, S. Baroni, Advanced capabilities for materials modelling with Quantum ESPRESSO, *J. Phys.: Condens. Matter.* 29 (2017) 465901, <http://dx.doi.org/10.1088/1361-648X/aa8f79>.
- [25] J.P. Perdew, K. Burke, M. Ernzerhof, Generalized gradient approximation made simple, *Phys. Rev. Lett.* 77 (18) (1996) 3865–3868, <http://dx.doi.org/10.1103/PhysRevLett.77.3865>.
- [26] D. Vanderbilt, Soft self-consistent pseudopotentials in a generalized eigenvalue formalism, *Phys. Rev. B* 41 (1990) 7892–7895, <http://dx.doi.org/10.1103/PhysRevB.41.7892>.
- [27] UltraSoft pseudopotentials for H, O, and Al atoms were taken from the Quantum ESPRESSO pseudopotential download page, 2024, <http://www.quantum-espresso.org/pseudopotentials> (files: H.pbe-rrkjus.UPF, O.pbe-rrkjus.UPF, Al.pbe-rrkjus_psl.0.1.UPF).
- [28] M. Methfessel, A.T. Paxton, High-precision sampling for Brillouin-zone integration in metals, *Phys. Rev. B* 40 (1989) 3616–3621, <http://dx.doi.org/10.1103/PhysRevB.40.3616>.
- [29] H.J. Monkhorst, J.D. Pack, Special points for Brillouin zone integrations, *Phys. Rev. B* 13 (1976) 5188–5192, <http://dx.doi.org/10.1103/PhysRevB.13.5188>.
- [30] P.E. Blöchl, Projector augmented-wave method, *Phys. Rev. B* 50 (24) (1994) 17953–17979, <http://dx.doi.org/10.1103/PhysRevB.50.17953>.
- [31] PAW pseudopotentials for H, O, and Al atoms were taken from the Quantum ESPRESSO pseudopotential download page, 2024, <http://www.quantum-espresso.org/pseudopotentials> (files: H.pbe-kjpaw_psl.0.1.UPF, O.pbe-kjpaw.UPF, Al.pbe-n-kjpaw_psl.0.1.UPF).
- [32] W. Tang, E. Sanville, G. Henkelman, A grid-based Bader analysis algorithm without lattice bias, *J. Phys.: Condens. Matter.* 21 (8) (2009) 084204, <http://dx.doi.org/10.1088/0953-8984/21/8/084204>.
- [33] A. Arnaldsson, W. Tang, G. Henkelman, et al., Computer program for Bader charge analysis, 2024, available from <https://theory.cm.utexas.edu/henkelman/code/bader/>.
- [34] A. Kokalj, XCRYSDen—a new program for displaying crystalline structures and electron densities, *J. Mol. Graph. Model.* 17 (1999) 176–179, [http://dx.doi.org/10.1016/S1093-3263\(99\)00028-5](http://dx.doi.org/10.1016/S1093-3263(99)00028-5), code available from <http://www.xcrysden.org/>.
- [35] X.-G. Wang, A. Chaka, M. Scheffler, Effect of the environment on α -Al₂O₃(0001) surface structures, *Phys. Rev. Lett.* 84 (2000) 3650–3653, <http://dx.doi.org/10.1103/PhysRevLett.84.3650>.
- [36] L. Bengtsson, Dipole correction for surface supercell calculations, *Phys. Rev. B* 59 (19) (1999) 12301–12304, <http://dx.doi.org/10.1103/PhysRevB.59.12301>.
- [37] M.W. Finnis, Accessing the excess: An atomistic approach to excesses at planar defects and dislocations in ordered compounds, *Phys. Status Solidi A* 166 (1) (1998) 397–416, [https://onlinelibrary.wiley.com/doi/abs/10.1002/\(SICI\)1521-396X\(199803\)166:1%3C397::AID-PSSA397%3E3.0.CO;2-%23](https://onlinelibrary.wiley.com/doi/abs/10.1002/(SICI)1521-396X(199803)166:1%3C397::AID-PSSA397%3E3.0.CO;2-%23).
- [38] S. Baroni, S. de Gironcoli, A. Dal Corso, P. Giannozzi, Phonons and related crystal properties from density-functional perturbation theory, *Rev. Modern Phys.* 73 (2001) 515, <http://dx.doi.org/10.1103/RevModPhys.73.515>.
- [39] R.F. Ribeiro, A.V. Marenich, C.J. Cramer, D.G. Truhlar, Use of solution-phase vibrational frequencies in continuum models for the free energy of solvation, *J. Phys. Chem. B* 115 (49) (2011) 14556–14562, <http://dx.doi.org/10.1021/jp205508z>.
- [40] M. Poberžnik, D. Costa, A. Hemeryck, A. Kokalj, Insight into the bonding of silanols to oxidized aluminum surfaces, *J. Phys. Chem. C* 122 (17) (2018) 9417–9431, <http://dx.doi.org/10.1021/acs.jpcc.7b12552>.
- [41] C. Lanthony, J. Ducéré, M.D. Rouhani, A. Hemeryck, A. Estève, C. Rossi, On the early stage of aluminum oxidation: An extraction mechanism via oxygen cooperation, *J. Chem. Phys.* 137 (9) (2012) 094707, <http://dx.doi.org/10.1063/1.4746943>.
- [42] V.A. Ranea, W.F. Schneider, I. Carmichael, DFT characterization of coverage dependent molecular water adsorption modes on α -Al₂O₃(0001), *Surf. Sci.* 602 (1) (2008) 268–275, <http://dx.doi.org/10.1016/j.susc.2007.10.029>.
- [43] G. Carchini, M. García-Melchor, Z. Łodziana, N. López, Understanding and tuning the intrinsic hydrophobicity of rare-earth oxides: A DFT+U study, *ACS Appl. Mater. Inter.* 8 (1) (2016) 152–160, <http://dx.doi.org/10.1021/acami.5b07905>.
- [44] V.A. Ranea, I. Carmichael, W.F. Schneider, DFT investigation of intermediate steps in the hydrolysis of α -Al₂O₃(0001), *J. Phys. Chem. C* 113 (6) (2009) 2149–2158, <http://dx.doi.org/10.1021/jp8069892>.
- [45] T. Bauer, T. Schmaltz, T. Lenz, M. Halik, B. Meyer, T. Clark, Phosphonate- and carboxylate-based self-assembled monolayers for organic devices: A theoretical study of surface binding on aluminum oxide with experimental support, *ACS Appl. Mater. Inter.* 5 (13) (2013) 6073–6080, <http://dx.doi.org/10.1021/am4008374>.